Distribution Agreement

In presenting this thesis as a partial fulfillment of the requirements for a degree from Emory University, I hereby grant to Emory University and its agents the non-exclusive license to archive, make accessible, and display my thesis in whole or in part in all forms of media, now or hereafter know, including display on the World Wide Web. I understand that I may select some access restrictions as part of the online submission of this thesis. I retain all ownership rights to the copyright of the thesis. I also retain the right to use in future works (such as articles or books) all or part of this thesis.

Carli B. Kovel April 10, 2018

Modulating the Catalytic Activity of First-Row Transition Metal Complexes Supported by Redox-Active Ligand Scaffolds

by

Carli B. Kovel

Dr. Cora E. MacBeth
Advisor

Department of Chemistry

Cora E. MacBeth
Advisor

Simon Blakey
Committee Member

Antonio Brathwaite
Committee Member

Christine Ristaino
Committee Member

2018

Modulating the Catalytic Activity of First-Row Transition Metal Complexes Supported by Redox-Active Ligand Scaffolds

by

Carli B. Kovel

Dr. Cora E. MacBeth

Advisor

An abstract of
a thesis submitted to the Faculty of Emory College of Arts and Sciences
of Emory University in partial fulfillment of the requirements of the degree
of Bachelor of Arts with Honors

Department of Chemistry

2018

Abstract

Modulating the Catalytic Activity of First-Row Transition Metal Complexes Supported by Redox-Active Ligand Scaffolds

By Carli B. Kovel

To pursue alternatives to the environmentally detrimental and toxic second- and third-row transition metal catalysts currently utilized in industry, the development of highly-efficient first-row transition metal catalysts for aerobic catechol oxidation and oxidative coupling were pursued in this work. Two redox-active ligands, *N*-(2-(phenylamino)phenyl)isobutyramide (H_2L^{iPr}) and 1-(*tert*-butyl)-3-(2-(phenylamino)phenyl)urea (H_3L^{Urea}) were synthesized and characterized. Cobalt(II), copper(II), and zinc(II) complexes ($[M(L^{iPr})_2]^{2-}$ and $[M(HL^{Urea})_2]^{2-}$) supported by each of the two ligand scaffolds were synthesized and characterized. X-ray diffraction data demonstrated that each ligand system stabilizes the mononuclear cobalt(II), copper(II), and zinc(II) complexes in a distorted tetrahedral geometry. Electrochemical properties of the complexes were examined through cyclic voltammetry which showed three reversible electrochemical events for each copper(II) complex and two reversible electrochemical events for each cobalt(II) and zinc(II) complex. When exposed to dioxygen, the six complexes presented herein catalytically oxidize 3,5-Di-*tert*-butylcatechol to 3,5-Di-*tert*-butyl-*o*-quinone. Cobalt(II) and copper(II) complexes supported by H_2L^{iPr} and H_3L^{Urea} ligand scaffolds were shown to aerobically catalyze oxidative phenolate coupling reactions, resulting in a biphenyl product.

.

Modulating the Catalytic Activity of First-Row Transition Metal Complexes Supported by Redox-Active Ligand Scaffolds

by

Carli B. Kovel

Dr. Cora E. MacBeth

Advisor

A thesis submitted to the Faculty of Emory College of Arts and Sciences
of Emory University in partial fulfillment
of the requirements of the degree
of Bachelor of Arts with Honors

Department of Chemistry

2018

Acknowledgements

I would like to thank everyone who helped me write my thesis. Dr. Cora MacBeth has provided me with invaluable guidance and support throughout my time at Emory University. She has pushed me to be a better chemist and researcher. I am so grateful that she has allowed me to be a part of her research group and that she introduced me to the field of inorganic chemistry. Dr. Savita Sharma has helped me develop my research skills and progress through this project. Sophie Cemaj has served as a mentor to me since the beginning of my time in the MacBeth group and her guidance has allowed me to understand the research process and develop new skills. She has always made research a joy. Dr. Omar Villanueva has taught new laboratory techniques and how to analyze data. I would also like to thank Dr. Simon Blakey for pushing me to understand my work at a deeper level and for helping me improve my reactions. Thank you to Dr. Tracy McGill for providing me with mentorship throughout my time at Emory and for inspiring me to pursue chemistry research. Additionally, I would like to thank Dr. Antonio Brathwaite for helping me improve my scientific writing. I would like to thank Dr. Christine Ristaino for her support and encouragement throughout my time at Emory. I would also like to thank the graduate students in the MacBeth group for their help with laboratory work and data collection. I am appreciative of everyone who helped contribute to this work and the progression of this project.

Table of Contents

Figures

Schemes

Tables

1. Introduction

Catalysis aims to increase molecular complexity and is widely employed in the pharmaceutical industry, fine chemicals industry, and is utilized for the conversion of feedstock chemicals into commodity chemicals.[1] Catalysts increase the rate of reaction by providing alternative lower energy pathways. Ideal catalysts are highly efficient and selective.[2] Specific examples of reactions that utilize catalysts are oxidation reactions and coupling reactions to form new C-C bonds. The synthesis of antiviral medication indinavir (**Figure 1**) requires an oxidation step.[3] Additionally, losartan (**Figure 2**), an anti-hypertensive is synthesized through Suzuki cross-coupling.[4]

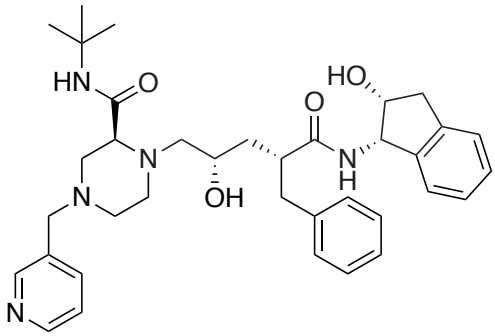

Figure 1: Chemical structure of indinavir.

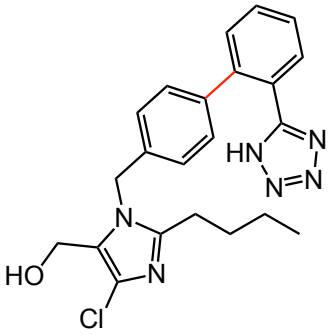

Figure 2: Chemical structure of losartan. The C-C bond highlighted in red is formed by Suzuki cross-coupling.

In the past, oxidative reactions in industry have employed toxic and wasteful synthetic methods including the use of alkyl and aryl halides as prefunctionalized substrates. The selective oxidation of alcohols required toxic oxidants including permanganates and chromates.[1] These expensive and wasteful stoichiometric processes are being replaced with catalytic processes that employ transition metal catalysts. Many of the transition metal catalysts currently used in industry utilize second- and third-row transition metals because they are able to facilitate multi-electron processes. Specifically, rhodium, iridium, and platinum are widely employed in transition metal catalyzed oxidation reactions.[5] These scarce elements are expensive, result in toxic by-products, and incur harm to the environment upon extraction from earth's crust.

The Shilov reaction is the first documented example of a platinum-catalyzed oxidation (**Scheme 1**). This selective oxidation of methane to methanol requires a stoichiometric oxidant, $PtCl_6^{2-}$. Another drawback of the reaction is that it needs to be heated to 120 °C.[6]

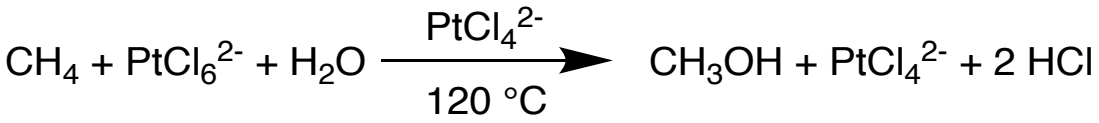

Scheme 1: The Shilov reaction.

Efforts to address the need for harmful and expensive stoichiometric oxidants, as well as high reaction temperatures have led to the use of palladium catalyzed oxidation reactions. Palladium(II) and palladium(IV) catalysts have still required stoichiometric oxidants including $PhI(OAc)_2$ and N-bromosuccinamide.[1] While these oxidants are both less expensive and toxic than the oxidant in the Shilov reaction, palladium is considered toxic to humans.[7]

Recently, Kozlowski, et al. reported ruthenium-catalyzed aerobic oxidative phenolic coupling.[8] While this reaction had a high yield of biphenyl products, it had to be carried out at 80

°C. Reactions that are able to occur at ambient conditions would be more environmentally benign. Additionally, ruthenium is a carcinogenic and expensive transition metal.[9]

To address the problems of wasteful oxidants and the use of precious metals, the MacBeth group has explored aerobic first-row transition metal catalysis. First-row transition metal are non-toxic, earth abundant, and inexpensive. One of the challenges of using first-row transition metals is their tendency to only facilitate one-electron processes. To address this problem, non-innocent and redox-active ligands have been designed to facilitate multi-electron processes when metallated to first-row transition metals.[5] We took a biomimetic approach, specifically examining catechol oxidase activities. The enzyme catechol oxidase catalyzes the aerobic oxidation of a catechol to the corresponding quinone (**Scheme 2**).[10] This oxidation is coupled to the reduction of molecular oxygen to water, the only by-product of this reaction.[11] The use of molecular oxygen as an oxidant is advantageous due to its low cost and lack of toxic by-products.[1] Metalloenzymes including catechol oxidase have been shown to operate under ambient conditions and display high selectivity.[12]

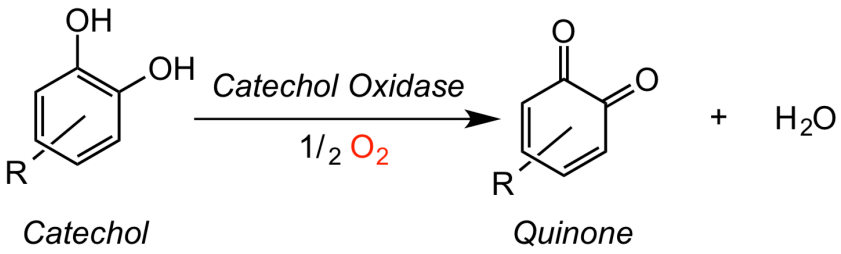

Scheme 2: Oxidation of catechol to quinone with molecular oxygen catalyzed by catechol oxidase.

Catechol oxidase belongs to the copper type-3 class of proteins, indicating the presence of two copper centers in its active site.[13] It has been documented that the oxidized form of catechol oxidase contains copper(II) centers (**Figure 3**) and the reduced form of the enzyme contains

copper(I) centers.[14] Each copper ion is surrounded by three histidine residues which act as nitrogen donors.[8] The active site of catechol oxidase has been documented to contain hydrogen-bond donors. These non-covalent interactions have been hypothesized to enhance catalytic reactivity.[15]

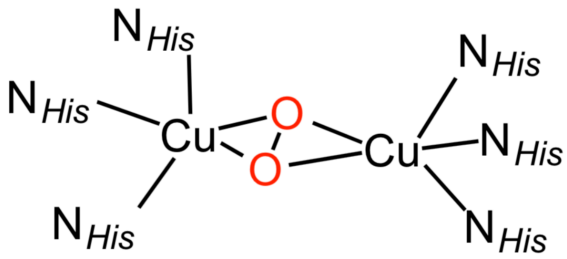

Figure 3: Oxidized form of the active site of the catechol oxidase enzyme.

Catechol oxidase activities are widely mimicked in the field of synthetic inorganic chemistry. Recent work has reported the use of binuclear first-row transition metal catalysts supported by ligands to selectively oxidize organic substrates. Work by Majumder, et al. has synthesized and shown the efficacy of mixed valent $Co^{III}Co^{II}$ complexes in mimicking catecholase activity.[16] While binuclear first-row transition metal complexes have been shown to be highly tunable and have been extensively researched, mononuclear complexes are favorable due to lower cost. Work by Gasque, et al. demonstrates considerable catecholase activity by copper complexes in which the two copper ions were too far of a distance from each other to be catalyzing the same substrate.[17] This finding indicated the possibility of utilizing mononuclear transition metal complexes for catechol oxidation.

In this work, the highly modular redox-active ligands *N*-(2-(phenylamino)phenyl)isobutyramide (H_2L^{iPr}) and 1-(*tert*-butyl)-3-(2-(phenylamino)phenyl)urea (H_3L^{Urea}), are synthesized, characterized, and metallated to copper(II), cobalt(II), and zinc(II) respectively. This work was done with the help of Dr. Omar Villanueva, Dr. Savita Sharma,

Jessica Elinburg, Sophie Cemaj, and Whitley Ramirez. H_3L^{Urea} contains hydrogen bond donors, providing the potential to stabilize the substrates and increase reactivity. This ligand was compared to H_2L^{iPr}, a similar ligand without hydrogen bond donors to determine the impact of hydrogen bond donors on catalytic reactivity. Characterization, ligand design, electrochemical profiles, and the reactivity of these novel complexes with dioxygen and 3,5-Di-*tert*-butylcatechol (3,5-DTBC) are discussed. 3,5-DTBC is a commonly studied substrate due to its low redox potential and its two-electron oxidation to the corresponding quinone is an accepted assessment of catecholase activity. A byproduct of utilizing molecular oxygen as an oxidant is water, so the use of activated molecular sieves to remove water and increase the rate of chemical conversion is also examined. The ability for our metal complexes to catalyze aerobic oxidative phenolic coupling was also explored in this work. All reactions catalyzed by our complexes were carried out at ambient temperature, further making these processes environmentally benign.

2. Results and Discussion

2.1 Synthesis and Characterization of Redox-Active Ligands

To investigate the impact of non-covalent interactions on first row transition metal complexes, we synthesized redox-active ligands H_2L^{iPr} and H_3L^{Urea}. H_2L^{iPr} was designed by Dr. Savita Sharma and H_3L^{Urea} was designed by Dr. Omar Villanueva. The ligand scaffolds have open coordination sites. Additionally, both ligand systems incorporate amidates into their structures, making their designs highly modular. The ligand scaffolds presented herein are air-stable, contrary related ligand scaffolds synthesized by Heyduk, et al. Heyduk and co-workers incorporated N,N′-bis(neo-pentyl)-ortho-phenylenediamide ligands into transition metal complexes.[18] These ligands were found to be air-sensitive. The amidate groups incorporated into the ligands in this work are reasoned to allow for stability under oxidizing conditions. Amidate

groups have been reported to be stable under oxidizing conditions.[19] Additionally, H_3L^{Urea} contains hydrogen-bond donors, allowing for potential inter and intramolecular-hydrogen bonding. This bio-inspired ligand design stems from the presence of hydrogen-bond donors in the active sites of metalloproteins.[15]

The synthetic routes of preparing H_2L^{iPr} and H_3L^{Urea} are displayed in **Scheme 3** and **Scheme 4** respectively. H_2L^{iPr} is synthesized in a one-step synthesis from the commercially available amine N-phenyl-o-phenylenediamine, which was acylated with isobutyryl chloride. To explore the effect of hydrogen-bond donors in the ligand scaffold, H_3L^{Urea} was generated from the same starting material. It was acylated with *tert*-butyl isocyanate.

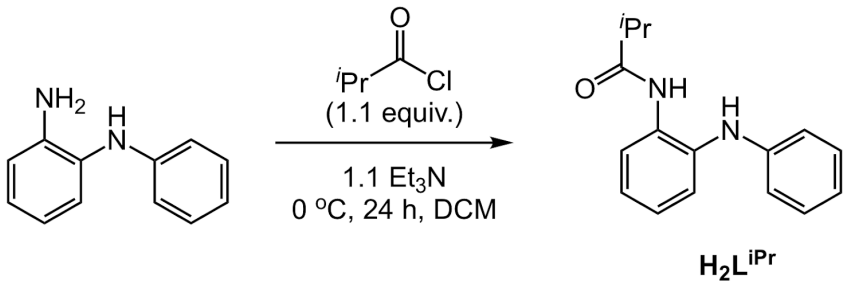

Scheme 3: Synthesis of redox-active ligand H_2L^{iPr}.

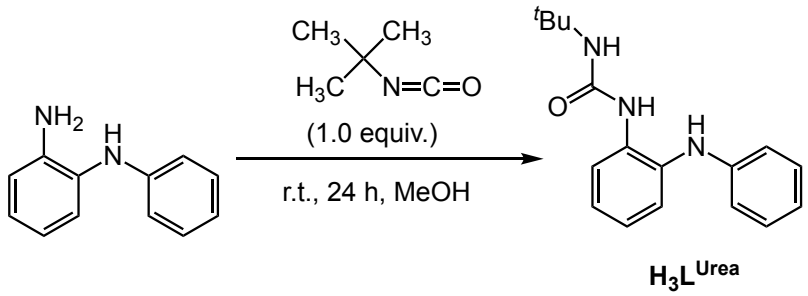

Scheme 4: Synthesis of redox-active ligand H_3L^{Urea}.

H_3L^{Urea} was characterized by ^1H NMR spectroscopy, mass spectrometry, and FTIR spectroscopy by Jessica Elinburg and Dr. Omar Villanueva. The ^1H NMR spectra exhibited two broad signals at 5.33 ppm and 6.32 ppm, which were determined to be characteristic of N-H signals. A third N-H signal was not observed which was attributed to an exchange with D_2O in solvent CD_3CN. The *tert*-butyl protons were observed at 1.29 ppm. In the mass spectrum, there was a peak at 284.00 m/z indicating 100% abundance of the 283.37 g/mol compound. The FTIR data displayed a characteristic C=O stretch at 1650 cm^{-1}. Three N-H stretches were displayed at 3385 cm^{-1}, 3372 cm^{-1}, and 3302 cm^{-1}. H_2L^{iPr} has been fully characterized by Dr. Savita Sharma.

2.2 Metal Complex Synthesis and Characterization

In this work, the metalation of H_2L^{iPr} and H_3L^{Urea} resulted in mononuclear cobalt(II), copper(II), and zinc(II) complexes. Past work in the MacBeth group has indicated that the nuclearity of complexes formed with the similar ligand H_3L^{iPr} was determined by the deprotonation of the ligand.[20] This premise was utilized in synthesizing the metal complexes presented herein. Additionally, unpublished work done by Dr. Omar Villanueva indicates that steric bulk may prevent the formation of dinuclear complexes. The six complexes: $[Co(L^{iPr})_2]^{2-}$, $[Cu(L^{iPr})_2]^{2-}$,$[Zn(L^{iPr})_2]^{2-}$, $[Co(HL^{Urea})_2]^{2-}$,$[Cu(HL^{Urea})_2]^{2-}$, and $[Zn(HL^{Urea})_2]^{2-}$ were synthesized under a nitrogen atmosphere due to the air-sensitive nature of the complexes. Immediately upon exposure to oxygen, all of the complexes were observed to undergo a color change. Counter ions for the metal complexes were chosen based on which resulted in the best crystals. Complexes with various counter ions including K^+, Et_4N^+, and PPh_4^+ were able to be synthesized and characterized. **Scheme 5** and **Scheme 7** display the counter ion exchange. The complex $K_2[Cu(HL^{Urea})_2]$ crystallized best without a counter ion exchange. The only by-products from the

two-step synthesis (**Schemes 5-7**) of these complexes were H_2 gas and KBr, indicating a low waste process.

$[M(HL^{Urea})_2]^{2-}$ complexes were characterized with the help of Dr. Omar Villanueva. We utilized FTIR and ^1H NMR spectroscopy, obtaining paramagnetic NMR spectra for cobalt (II) and copper (II) complexes. FTIR spectra consistently revealed stretches consistent with C=O and N-H stretches. FTIR data for $(Et_4N)_2[Co(HL^{Urea})_2]$, $K_2[Cu(HL^{Urea})_2]$, and $(Et_4N)_2[Zn(HL^{Urea})_2]$ is displayed in Table 1.

Table 1: Characteristic FTIR stretches for $(Et_4N)_2[Co(HL^{Urea})_2]$, $K_2[Cu(HL^{Urea})_2]$, and $(Et_4N)_2[Zn(HL^{Urea})_2]$.

Stretch	**$(Et_4N)_2[Co(HL^{Urea})_2]$**	**$K_2[Cu(HL^{Urea})_2]$**	**$(Et_4N)_2[Zn(HL^{Urea})_2]$**
$N–H_{amide}$	3314 cm^{-1}	3270 cm^{-1}	3277 cm^{-1}
C=O	1655 cm^{-1}	1676 cm^{-1}	1655 cm^{-1}

Paramagnetic ^1H NMR spectra were obtained for $(Et_4N)_2[Co(HL^{Urea})_2]$ and $K_2[Cu(HL^{Urea})_2]$. Each spectrum exhibited nine peaks as expected. The peaks correspond to the nine chemically inequivalent protons of the each of the two chemically equivalent ligands bound to each metal center. The peaks of each spectra displayed characteristic paramagnetic shifts. The ^1H NMR spectrum obtained for $K_2[Zn(HL^{Urea})_2]$ contained a peak at 0.98 ppm which was characteristic of the nine *tert*-butyl protons. There were signals between 6.5 and 8.0 ppm characteristic of the aromatic protons on the ligand scaffold.

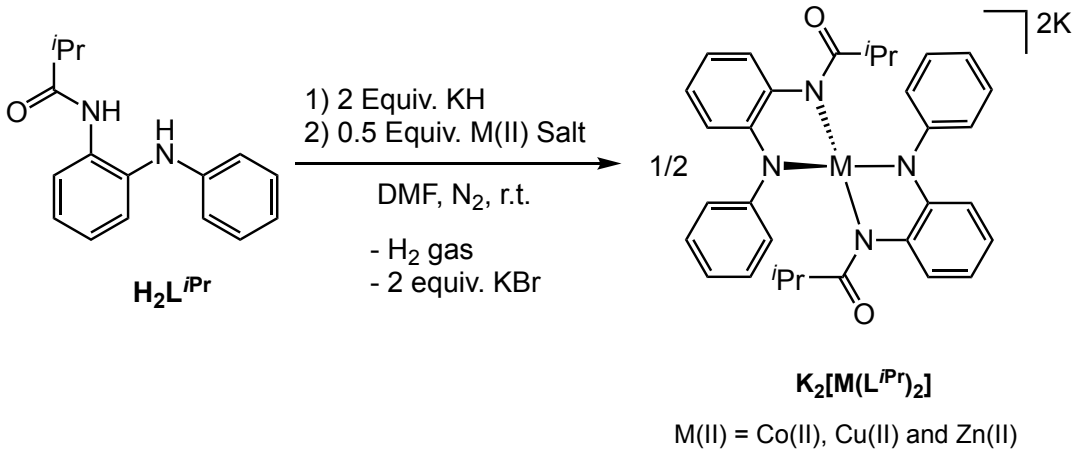

Scheme 5: Synthesis of $[M(L^{iPr})_2]^{2-}$ complexes.

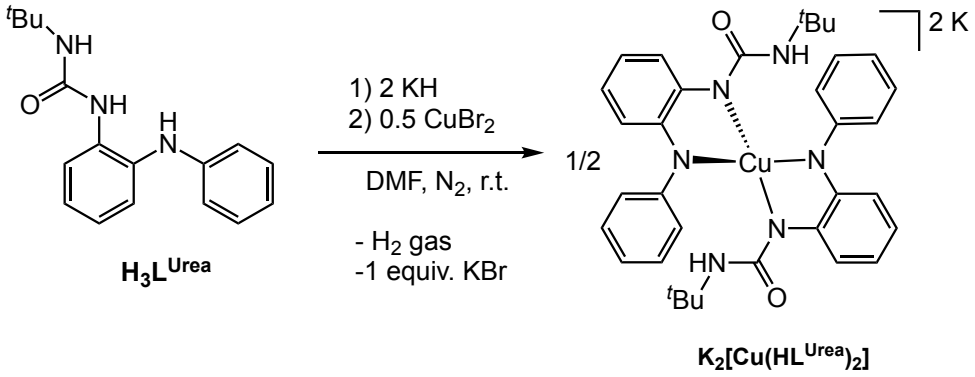

Scheme 6: Synthesis of $K_2[Cu(HL^{Urea})_2]$ complex.

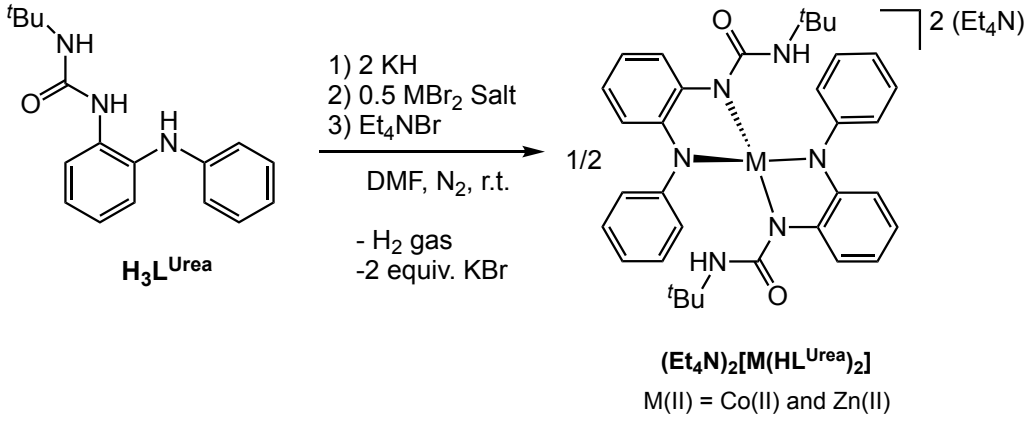

Scheme 7: Synthesis of $(Et_4N)_2[Co(HL^{Urea})_2]$ and $(Et_4N)_2[Zn(HL^{Urea})_2]$ complexes.

2.3 Crystallographic Characterization of Metal Complexes

The metal complexes presented herein were able to be crystallized into X-ray diffraction quality crystals through layering techniques as well as via slow diffusion of diethyl ether into an acetonitrile solution of the respective metal complex. $(Et_4N)_2[Co(HL^{Urea})_2]$ was crystallized into dark red blocks, $K_2[Cu(HL^{Urea})_2]$ crystals were dark aqua blocks, and $(Et_4N)_2[Zn(HL^{Urea})_2]$ was crystallized to dark yellow blocks. $(PPh_4)_2[Co(L^{iPr})_2]$ was crystalized into dark red blocks, while $(Et_4N)_2[Zn(L^{iPr})_2]$ crystals were yellow blocks.

Crystal structures of $(PPh_4)_2[Co(L^{iPr})_2]$, $(Et_4N)_2[Cu(L^{iPr})_2]$, $(Et_4N)_2[Zn(L^{iPr})_2]$, $(Et_4N)_2[Co(HL^{Urea})_2]$, $K_2[Co(HL^{Urea})_2]$, and $(PPh_4)_2[Co(HL^{Urea})_2]$ were obtained using X-ray diffraction. Crystal structures of $(PPh_4)_2[Co(L^{iPr})_2]$, $(Et_4N)_2[Cu(L^{iPr})_2]$, and $(Et_4N)_2[Zn(L^{iPr})_2]$ were obtained by Dr. Savita Sharma. The crystal structures of $(Et_4N)_2[Co(HL^{Urea})_2]$, $K_2[Co(HL^{Urea})_2]$, and $(PPh_4)_2[Co(HL^{Urea})_2]$ were obtained by Dr. Omar Villanueva and Jessica Elinburg. Notable bond lengths for $(PPh_4)_2[Co(L^{iPr})_2]$ and $(Et_4N)_2[Zn(L^{iPr})_2]$ complexes are presented in **Table 2**. These structures exhibited a four-coordinate distorted tetrahedral geometry, with τ_4 values of 0.74 and 0.8 for $(PPh_4)_2[Co(L^{iPr})_2]$ and $(Et_4N)_2[Zn(L^{iPr})_2]$ respectively. $(Et_4N)_2[Cu(L^{iPr})_2]$ also exhibited four-coordinate distorted tetrahedral geometry. However, the data for this complex is not included in this work.

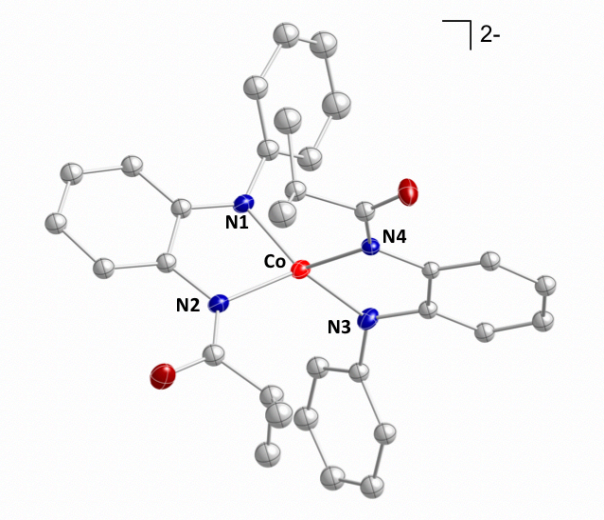

Figure 4: Solid-state structure of $(PPh_4)_2[Co(L^{iPr})_2]$.

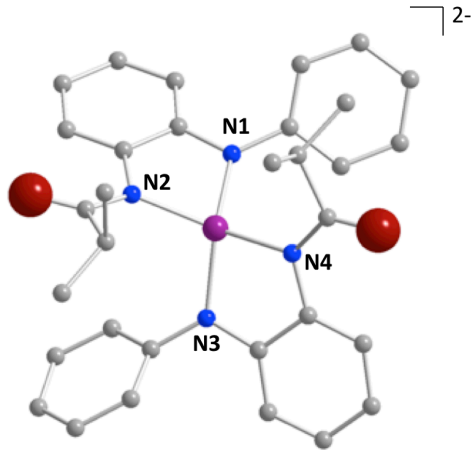

Figure 5: Solid-state structure of $(PPh_4)_2[Cu(L^{iPr})_2]$.

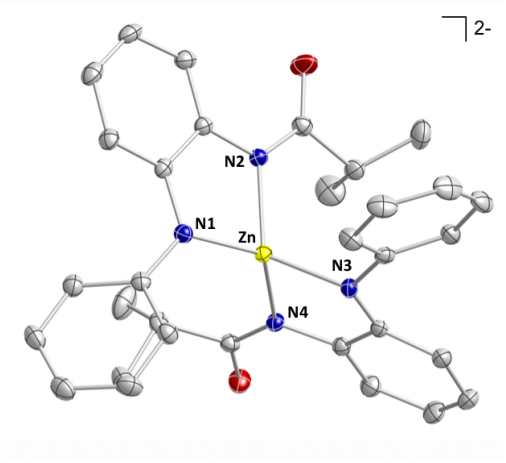

Figure 6: Solid-state structure of $(Et_4N)_2[Zn(L^{iPr})_2]$.

Table 2: Notable bond lengths and angles for $(PPh_4)_2[Co(L^{iPr})_2]$ and $(Et_4N)_2[Zn(L^{iPr})_2]$ complexes.

Parameter	**$(PPh_4)_2[Co(L^{iPr})_2]$**	**$(Et_4N)_2[Zn(L^{iPr})_2]$**
$M–N_{amide}$	1.9775(5) Å	1.985(2) Å
$M–N_{amidate}$	2.020(6) Å	2.002(3) Å
$N_{amido}–M–N_{amidate}$	82.8(2)°	84.75(8)°
$N_{amidate}–M–N_{amidate}$	117.6(2)°	117.34(8)°
$N_{amido}–M–N_{amido}$	129.3(2)°	128.66(8)°

Crystal structures obtained for of $(Et_4N)_2[Co(HL^{Urea})_2]$,$K_2[Cu(HL^{Urea})_2]$, and $(Et_4N)_2[Zn(HL^{Urea})_2]$ all adopted a four-coordinate distorted tetrahedral geometry. The τ_4 values for $(Et_4N)_2[Co(HL^{Urea})_2]$,$K_2[Cu(HL^{Urea})_2]$, and $(Et_4N)_2[Zn(HL^{Urea})_2$ were 0.63, 0.51, and 0.73 respectively. Important angles and bond lengths are noted in **Table 3**.

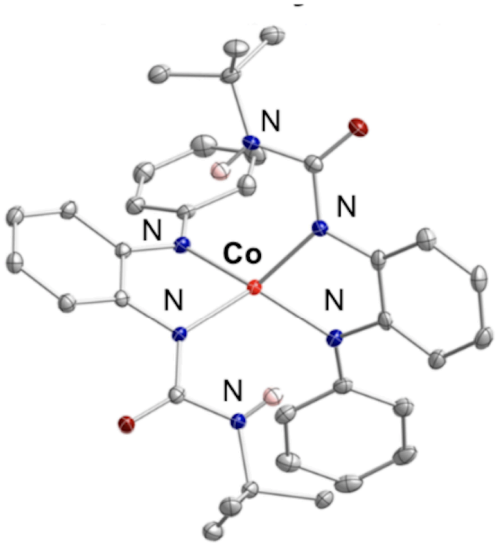

Figure 7: Solid-state structure of $(Et_4N)_2[Co(HL^{Urea})_2]$.

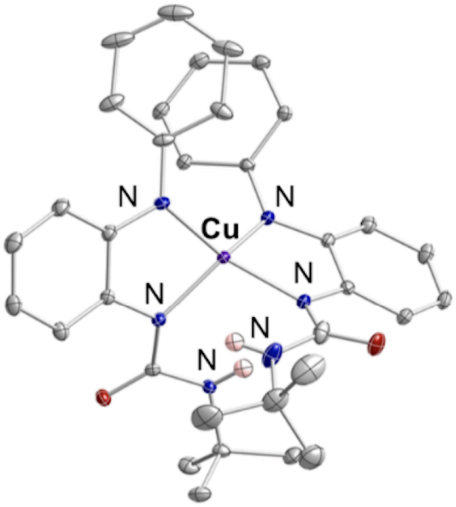

Figure 8: Solid-state structure of $K_2[Cu(HL^{Urea})_2]$.

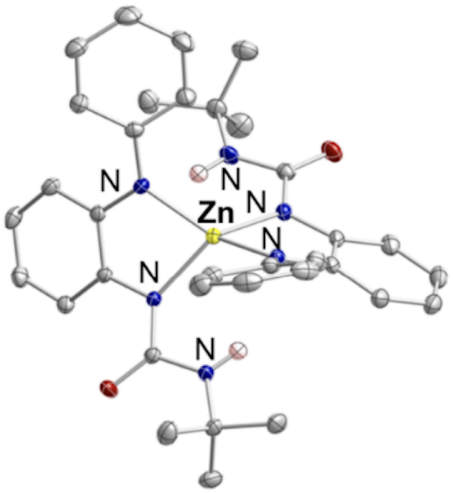

Figure 9: Solid-state structure of $(Et_4N)_2[Zn(HL^{Urea})_2]$.

Table 3: Notable bond lengths and angles for $(Et_4N)_2[Co(HL^{Urea})_2]$, $K_2[Cu(HL^{Urea})_2]$, and $(Et_4N)_2[Zn(HL^{Urea})_2]$.

Parameter	**$(Et_4N)_2[Co(HL^{Urea})_2]$**	**$K_2[Cu(HL^{Urea})_2]$**	**$(Et_4N)_2[Zn(HL^{Urea})_2]$**
$M–N_{amide}$	1.99(3) Å	1.94(13) Å	1.99(2) Å
$M–N_{amidate}$	2.00(3) Å	1.98(13) Å	2.02(6) Å
$N_{amido}–M–N_{amidate}$	82.57(12)°	83.63(5)°	83.01(10)°
$N_{amidate}–M–N_{amidate}$	130.74(11)°	103.19(5)°	126.00(10)°
$N_{amido}–M–N_{amido}$	140.29(12)°	110.80(6)°	142.12(11)°

The distorted tetrahedral geometries of the five complexes noted were determined by the τ_4 values which correspond to four-coordinate geometries on a scale from 0.00-1.00, in which 0.00 is square planar and 1.00 is tetrahedral. This scale was proposed by Houser, et al. and utilizes the bond angles of the coordination sphere to quantify the geometry of four-coordinate species.[21] The structures of all of the metal complexes were similar, indicating that highly modular amidate ligands may stabilize four-coordinate distorted tetrahedral geometry in various first row transition metal complexes. Additionally, the similar geometries of the complexes further indicate that the altered substituent on the amide group of the ligand does not significantly change the coordination geometry of the complexes presented herein.

2.4 Electrochemical Characterization of Metal Complexes

We explored the electrochemical properties of the metal complexes through cyclic voltammetry. Electrochemical data for the complexes $(PPh_4)_2[Co(L^{iPr})_2]$, $Et_4N)_2[Cu(L^{iPr})_2]$, and $(Et_4N)_2[Zn(L^{iPr})_2]$ was obtained by Dr. Savita Sharma. Electrochemical data for $(Et_4N)_2[Co(HL^{Urea})_2]$, $K_2[Cu(HL^{Urea})_2]$, and $(Et_4N)_2[Zn(HL^{Urea})_2]$ was collected by Dr. Omar Villanueva. The electrochemical properties of our metal complexes were explored via cyclic voltammetry. Each complex displayed multiple reversible electrochemical events. This finding contrasted to past unpublished work with isopropyl substituted complexes done in the MacBeth group which found irreversible electrochemical responses for binuclear cobalt complexes. This work on dinuclear complexes $(PPh_4)_2[Fe_2(L^{iPr})_2]$, $(Et_4N)_2[Ni_2(L^{iPr})_2]$, and $(Et_4N)_2[Zn_2(L^{iPr})_2]$ was conducted by Dr. Omar Villanueva.

Complexes $(PPh_4)_2[Co(L^{iPr})_2]$, $(PPh_4)_2[Cu(L^{iPr})_2]$, $(Et_4N)_2[Zn(L^{iPr})_2]$ displayed rich electrochemical profiles. $(PPh_4)_2[Co(L^{iPr})_2]$ displayed two reversible electrochemical events at -

1.126 V and -0.66 V. Similarly, $(Et_4N)_2[Zn(L^{iPr})_2]$ also displayed two reversible electrochemical events at -0.894 V and -0.590 V. $(PPh_4)_2[Cu(L^{iPr})_2]$ displayed three different electrochemical events at -1.107 V, -0.651 V, and -0.127 V. Since zinc(II) is a redox-inactive metal, the two reversible electrochemical responses were from the redox-active ligand backbone, not the metal center. The two electrochemical events displayed by $(PPh_4)_2[Co(L^{iPr})_2]$ can be attributed to the redox active ligand as a result. Since $(PPh_4)_2[Cu(L^{iPr})_2]$ displayed three reversible electrochemical events, one of these events must occur at the metal center. Additionally, $(PPh_4)_2[Co(L^{iPr})_2]$ had the most negative redox potential, indicating that it is the most easily oxidized of the three complexes.

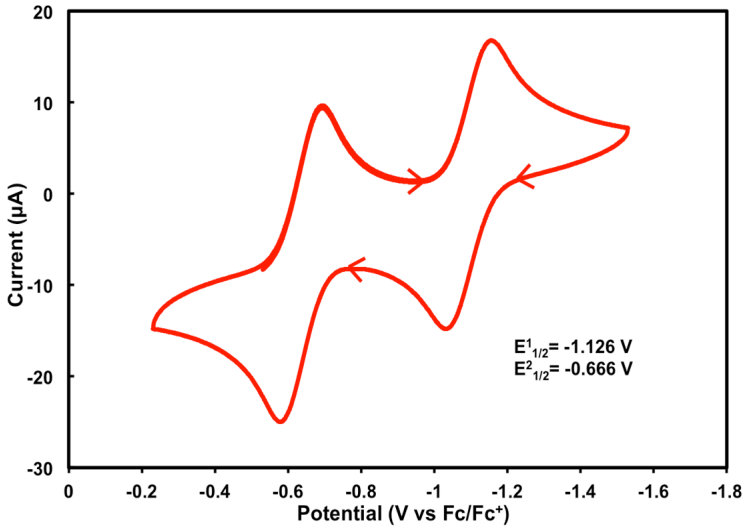

Figure 10: Cyclic voltammogram of $(PPh_4)_2[Co(L^{iPr})_2]$ under the following conditions: 10 mV/s, 0.1 M tetrabutylammonium hexafluorophosphate ($TBAPF_6$) supporting electrolyte, solvent was dichloromethane, referenced against Fc/Fc^+, with Ag/Ag^+ as reference electrode, glassy carbon working electrode.

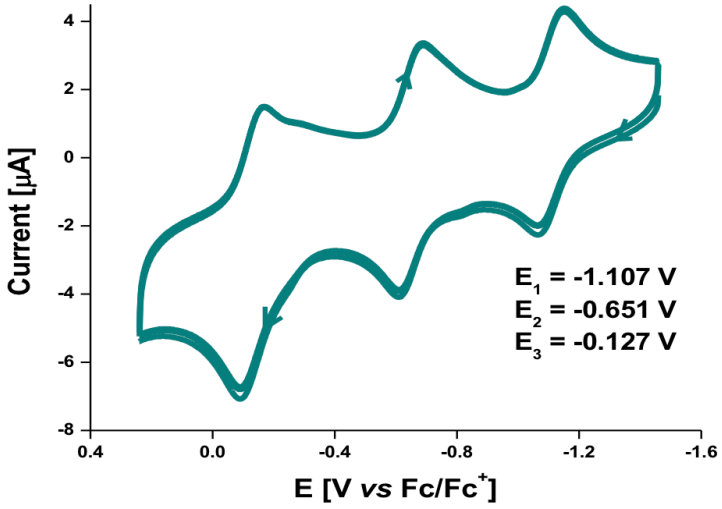

Figure 11: Cyclic voltammogram of $(PPh_4)_2[Cu(L^{iPr})_2]$ under the following conditions: 0.1 M tetrabutylammonium hexafluorophosphate ($TBAPF_6$) supporting electrolyte, solvent was dichloromethane, referenced against Fc/Fc^+, with Ag/Ag^+ as reference electrode, glassy carbon working electrode.

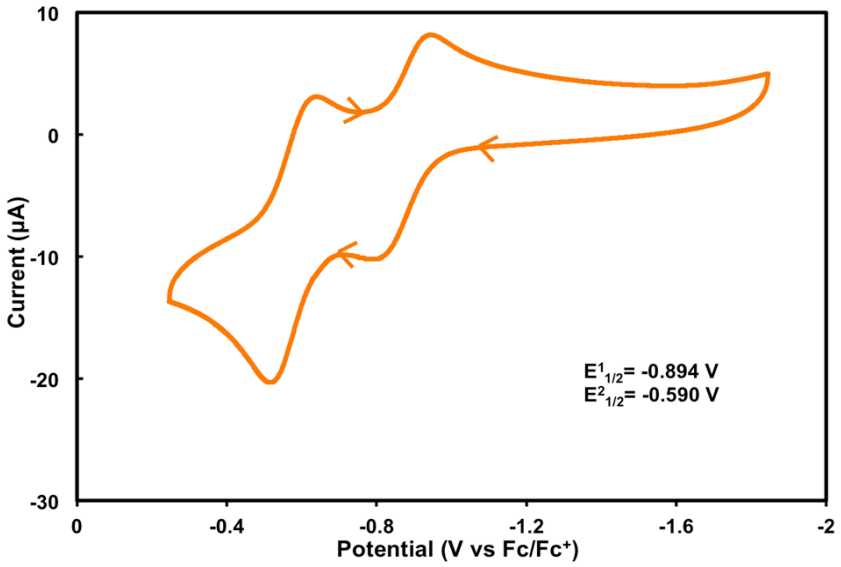

Figure 12: Cyclic voltammogram of $(Et_4N)_2[Zn(L^{iPr})_2]$ under the following conditions: 0.1 M tetrabutylammonium hexafluorophosphate ($TBAPF_6$) supporting electrolyte, solvent was dichloromethane, referenced against Fc/Fc^+, with Ag/Ag^+ as reference electrode, glassy carbon working electrode.

Cyclic voltammograms for $(Et_4N)_2[Co(HL^{Urea})_2]$ and $(Et_4N)_2[Zn(HL^{Urea})_2]$ each displayed two reversible electrochemical events. The events for $(Et_4N)_2[Co(HL^{Urea})_2]$ occurred at -1.282 V and -0.411 V. The reversible electrochemical events for $(Et_4N)_2[Zn(HL^{Urea})_2]$ were at -0.975 V and -0.568 V. The cyclic voltammogram for $K_2[Cu(HL^{Urea})_2]$ showed three reversible electrochemical events at -1.235 V, -0.791 V, and -0.328 V. The two reversible electrochemical events displayed on the cyclic voltammogram of $(Et_4N)_2[Zn(HL^{Urea})_2]$ indicate that H_3L^{Urea} is redox-active. The reversible electrochemical events displayed by the $(Et_4N)_2[Co(HL^{Urea})_2]$ complex likely occurred at the redox-active ligand backbone. Since $K_2[Cu(HL^{Urea})_2]$ displayed three reversible electrochemical events, one of these events likely occurred at the metal center. Additionally, $(Et_4N)_2[Co(HL^{Urea})_2]$ had the most negative redox potential, indicating that it is easier to oxidize than $K_2[Cu(HL^{Urea})_2]$ and $(Et_4N)_2[Zn(HL^{Urea})_2]$. When comparing the metal

complexes supported by H_2L^{iPr} and H_3L^{Urea}, the metal complexes supported by redox-active ligand H_3L^{Urea} displayed lower redox potentials. This indicates that the hydrogen-bond donors incorporated into the redox-active ligand scaffold allow the metal complexes to be easier to oxidize.

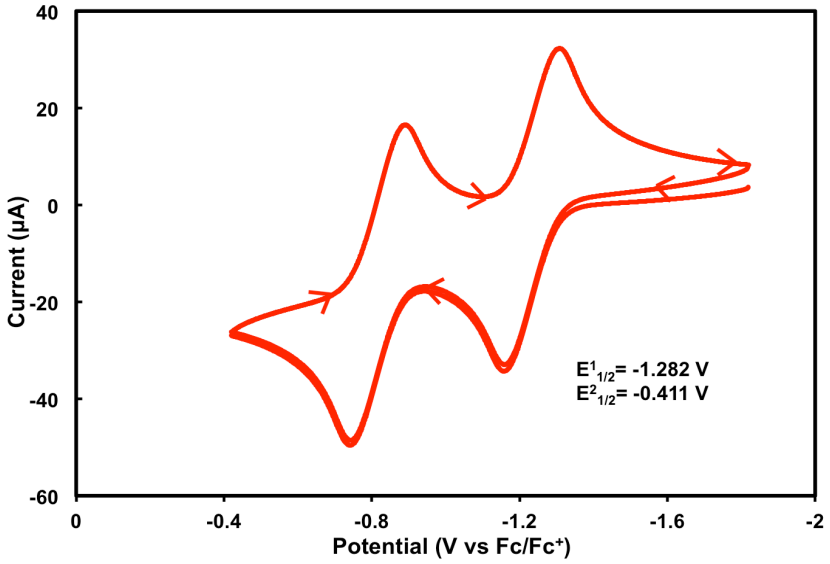

Figure 13: Cyclic voltammogram of $(Et_4N)_2[Co(HL^{Urea})_2]$ under the following conditions: 0.1 M tetrabutylammonium hexafluorophosphate ($TBAPF_6$) supporting electrolyte, solvent was dichloromethane, referenced against Fc/Fc^+, with Ag/Ag^+ as reference electrode, glassy carbon working electrode.

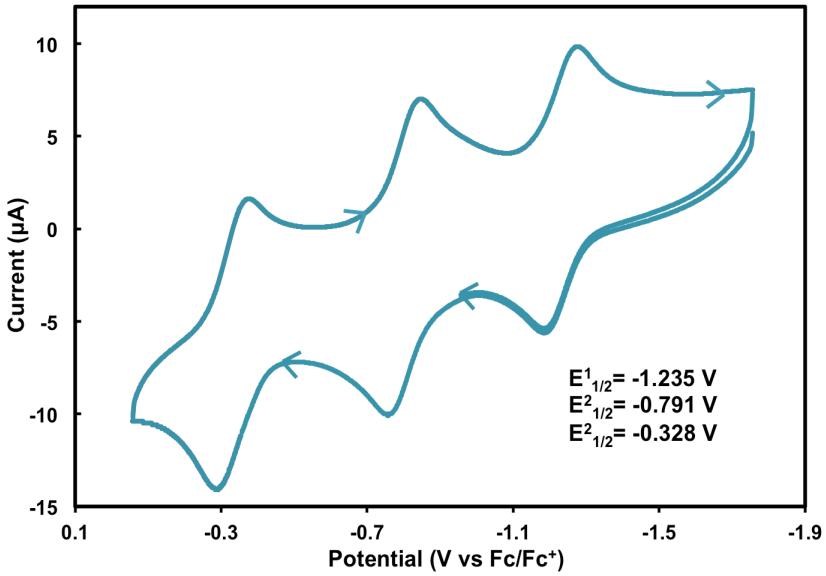

Figure 14: Cyclic voltammogram of $K_2[Cu(HL^{Urea})_2]$ under the following conditions: 0.1 M tetrabutylammonium hexafluorophosphate ($TBAPF_6$) supporting electrolyte, solvent was dichloromethane, referenced against Fc/Fc^+, with Ag/Ag^+ as reference electrode, glassy carbon working electrode.

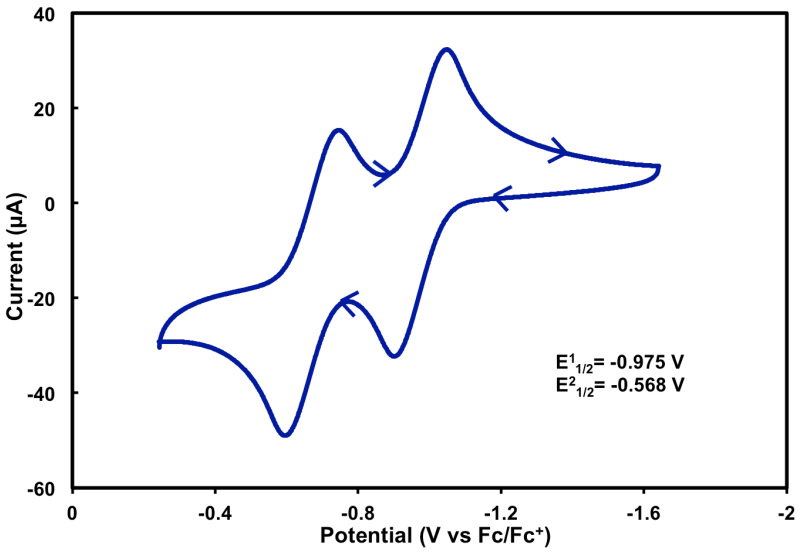

Figure 15: Cyclic voltammogram of $(Et_4N)_2[Zn(HL^{Urea})_2]$ under the following conditions: 0.1 M tetrabutylammonium hexafluorophosphate ($TBAPF_6$) supporting electrolyte, solvent was dichloromethane, referenced against Fc/Fc^+, with Ag/Ag^+ as reference electrode, glassy carbon working electrode.

2.5 Monitoring Catechol Oxidation with UV-Visible Spectroscopy

We explored the ability of our complexes to utilize molecular oxygen to oxidize catechol to quinone. The reaction was carried out according to Scheme 8 for $(PPh_4)_2[Co(HL^{Urea})_2]$ and $(PPh_4)_2[Co(L^{iPr})_2]$ to explore the *in-situ* reactivity of the complexes. 3,5-DTBC is a commonly used substrate when examining catecholase activity due to its low redox potential.[22] Additionally, a catechol with bulky *tert*-butyl substituents was utilized to prevent other reactions from occurring. The tert-butyl groups also have the ability to stabilize the potential radical formed during this reaction.

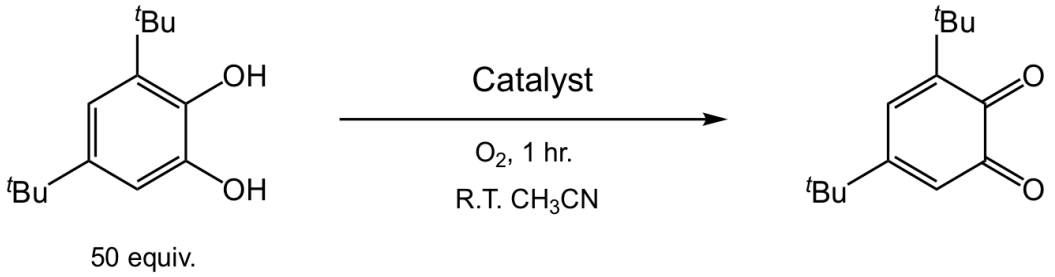

Scheme 8: Oxidation of 3,5-DTBC to 3,5-DTBQ facilitated by $(PPh_4)_2[Co(HL^{Urea})_2]$ and $(PPh_4)_2[Co(L^{iPr})_2]$. The reaction was monitored by UV-Visible spectroscopy.

The formation of the 3,5-Di-tert-butylquinone (3,5-DTBQ) product was displayed by the characteristic absorbance bands at approximately 400 nm.[23] No intermediates were observed, indicated by the single peak observed in each spectrum. The isosbestic point was observed at approximately 325 nm in each spectrum. $(PPh_4)_2[Co(HL^{Urea})_2]$ and $(PPh_4)_2[Co(L^{iPr})_2]$ displayed similar spectra.

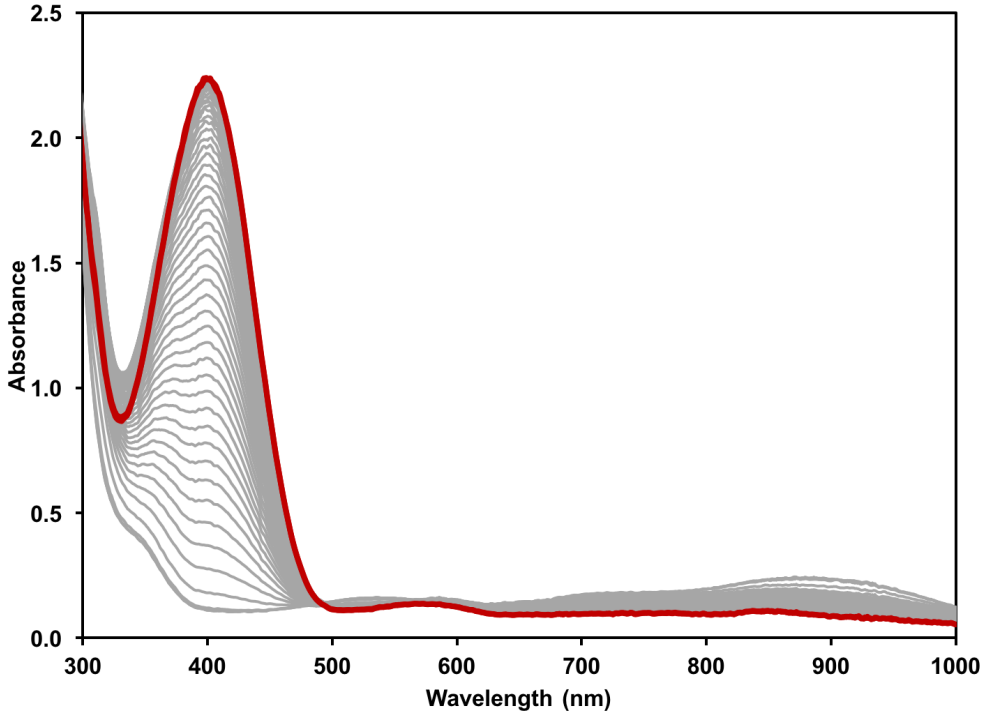

Figure 16: UV-Visible absorption spectra of the oxidation of 50 equivalents of 3,5-DTBC to 3,5-DTBQ facilitated by 1.0 equivalent of $(PPh_4)_2[Co(L^{iPr})_2]$. Spectra was obtained at ambient temperature in acetonitrile with a scan rate of 1 scan/minute.

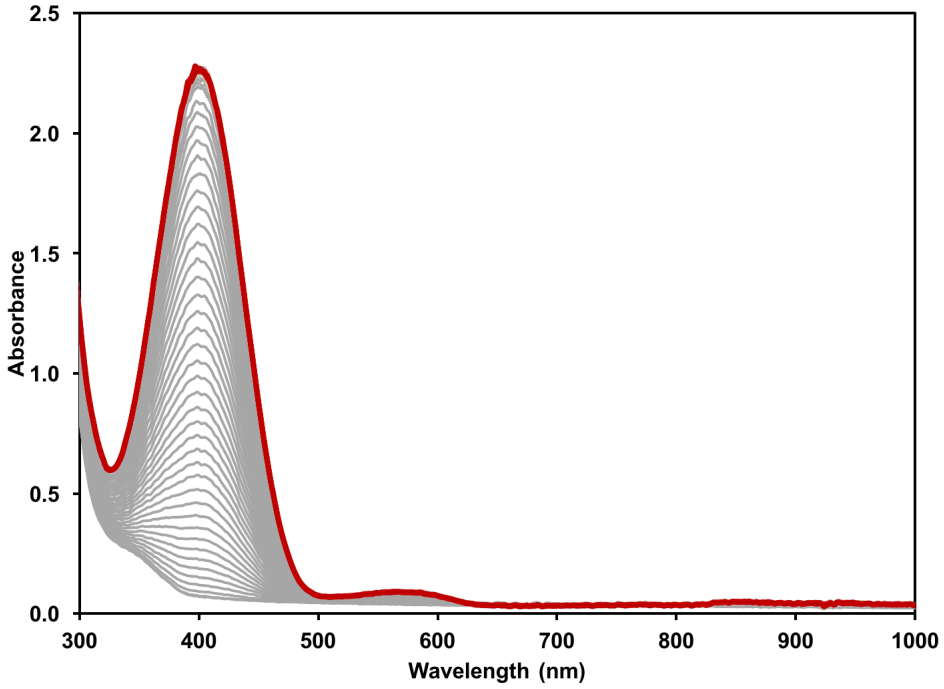

Figure 17: UV-Visible absorption spectra of the oxidation of 50 equivalents of 3,5-DTBC to 3,5-DTBQ facilitated by 1.0 equivalent of $(PPh_4)_2[Co(HL^{Urea})_2]$. Spectra was obtained at ambient temperature in acetonitrile with a scan rate of 1 scan/minute.

2.6 Reactivity Studies of Catechol Oxidation

The main goal of our research is to use our metal complexes as a catalyst to perform aerobic oxidation of catechol in catalytic amount. General catalytic aerobic substrate oxidation procedures were followed for these experiments. We first carried out control reactions. The catechol was dissolved in acetonitrile and exposed to pure oxygen for 2 hours. No product was formed. We also carried out other control reaction where we only utilized metal salt instead of our catalyst. From ^1H NMR, it was determined that no product was formed and we were left with only starting material. Our findings indicated that a metal complex supported by a redox-active ligand scaffold was necessary to convert starting material to product. Additionally, our metal complexes catalyzed the conversion of catechol to quinone at ambient temperature. The mild

conditions in which our complexes are able to catalyze reactions are favorable for environmentally benign processes.

To understand the impact of the redox-active ligand scaffolds on catalytic activity, we compared turnover numbers (TON) which are shown in **Table 4**. Cobalt(II) complex $(PPh_4)_2[Co(L^{iPr})_2]$ only converted 45% of 3,5-DTBC to 3,5-DTBQ in 2 hours, while $(PPh_4)_2[Co(HL^{Urea})_2]$ catalyzed the oxidation to completion, indicating its higher catecholase activity. Entries **5** and **6** demonstrate the enhanced catalytic activity of cobalt(II) complexes supported by ligands that incorporate hydrogen-bond donors. This trend was followed when comparing the TON of $(PPh_4)_2[Cu(L^{iPr})_2]$ to the TON of $K_2[Cu(HL^{Urea})_2]$. Of the zinc(II) complexes, $(Et_4N)_2[Zn(L^{iPr})_2]$ exhibited lower catalytic activity than $(PPh_4)_2[Zn(HL^{Urea})_2]$. The data collected for cobalt(II), copper(II), and zinc(II) metal complexes corroborates our hypothesis that ligand scaffolds that incorporate hydrogen-bond donor groups into the secondary coordination environment of the active site enhance catalytic activity.

Additionally, $(PPh_4)_2[Co(HL^{Urea})_2]$ exhibited the highest catalytic activity of each complex under the conditions noted in **Table 4**. No other metal complexes were observed to go to completion. $(PPh_4)_2[Co(L^{iPr})_2]$ exhibited the highest catalytic activity of the three metal complexes supported by H_2L^{iPr}, indicating that the cobalt(II) complexes synthesized in this work exhibited higher catalytic activity than the copper(II) and zinc(II) complexes. We expected the copper(II) complexes to exhibit higher reactivity due to the presence of copper ions in many metalloenzymes, including the active site of catechol oxidase.[13] This finding led us to focus the remainder of our studies on catechol oxidation on optimizing the reaction conditions for the conversion of 3,5-DTBC to 3,5-DTBQ catalyzed by cobalt(II) complexes.

Table 4: Oxidation of 3,5-DTBC to 3,5-DBBQ with $[M(L^{iPr})_2]^{2-}$ and $[M(HL^{Urea})_2]^{2-}$.

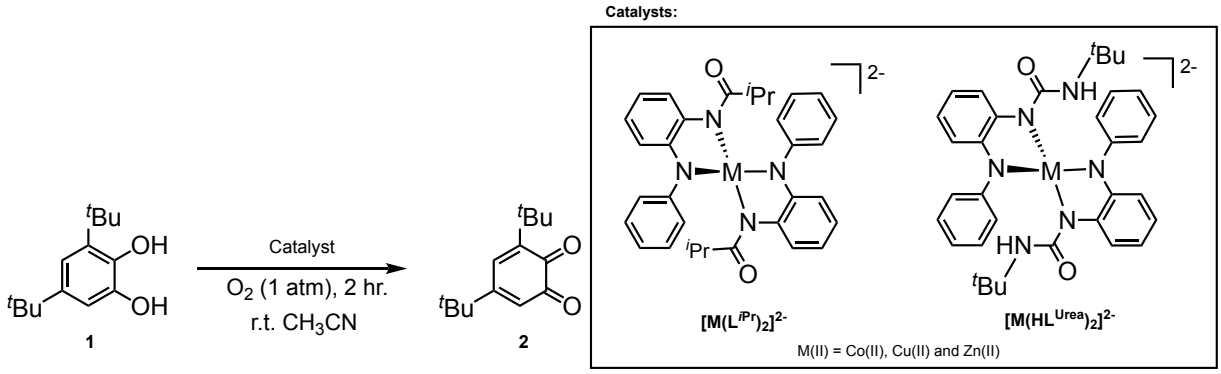

Entry	Catalyst	Cat.:Substrate Loading	% Conversion[a]	Isolated Yield of **2** (%)	TON
1	—	—	0	—	—
2	$CoBr_2$	1:50	0	—	—
3	$CuBr_2$	1:50	0	—	—
4	$ZnBr_2$	1:50	0	—	—
5	$(PPh_4)_2[Co(L^{iPr})_2]$	1:100	45	—	45[b]
6	$(PPh_4)_2[Co(HL^{Urea})_2]$	1:100	100	60	62[c]
7	$(PPh_4)_2[Cu(L^{iPr})_2]$	1:50	18	—	9[b]
8	$K_2[Cu(HL^{Urea})_2]$	1:50	90	—	46[b]
9	$(Et_4N)_2[Zn(L^{iPr})_2]$	1:50	25	—	13[b]
10	$(PPh_4)_2[Zn(HL^{Urea})_2]$	1:50	67	—	34[b]

[a] % Conversions were determined via ^1H NMR
[b] TON = (moles of product determined from % conversion / moles of catalyst)
[c] TON = (moles of product / moles of catalyst)

We hypothesized that a by-product of the catalytic aerobic oxidation of 3,5-DTBC was water. In the catechol oxidase enzyme, catechol oxidation is coupled to the 4-electron reduction of molecular oxygen to water. The formation of water could bind to the metal complexes and impede catalytic activity. To address this problem, we added activated molecular sieves to the reaction mixture. Control reactions were carried out utilizing our procedure for catalytic aerobic substrate oxidation, with the addition of 4 Å molecular sieves. Only starting material remained when no catalyst was used, as well as when $CoBr_2$ was utilized in place of a catalyst. These results indicate that even when molecular sieves were added to the reaction mixture, a metal

catalyst supported by a redox-active ligand scaffold was necessary for conversion to product in ambient conditions.

Since the catechol oxidation reaction catalyzed by $(PPh_4)_2[Co(HL^{Urea})_2]$ went to completion with a 1:100 catalyst:substrate loading without the addition molecular sieves, we increased the ratio to 1:150. Entry **5** in **Table 5** displays that $(PPh_4)_2[Co(HL^{Urea})_2]$ catalyzed the conversion of 3,5-DTBC to 3,5-DTBQ to completion in 2 hours. 3,5-DTBQ was collected in a high yield of 87%. To compare the two ligand scaffolds in the new reaction conditions, the same reaction was run for $(PPh_4)_2[Co(L^{iPr})_2]$. The percent conversion increased from 45% to 80% with the addition of molecular sieves and an increased catalyst:substrate loading. These results indicated that molecular sieves enhanced the catalytic activity of $(PPh_4)_2[Co(L^{iPr})_2]$, but the complex remained less efficient than $(PPh_4)_2[Co(HL^{Urea})_2]$. The enhanced reactivity observed when molecular sieves were added to the reaction mixture corroborated our hypothesis that water was formed as a by-product of the oxidation of 3,5-DTBC.

While continuing to add molecular sieves to the reaction, we further increased the catalyst:substrate loading to 1:500 and allowed the reaction to run for 24 hours. The oxidation catalyzed by $(PPh_4)_2[Co(HL^{Urea})_2]$ went to completion, while the oxidation catalyzed by $(PPh_4)_2[Co(L^{iPr})_2]$ only converted 63% of 3,5-DTBC to 3,5-DTBQ. In all trials conducted, $(PPh_4)_2[Co(HL^{Urea})_2]$ was the most reactive complex.

Table 5: Oxidation of 3,5-DTBC to 3,5-DTBQ with $(PPh_4)_2[Co(L^{iPr})_2]$and $(PPh_4)_2[Co(HL^{Urea})_2]$ with molecular sieves added to the reaction.

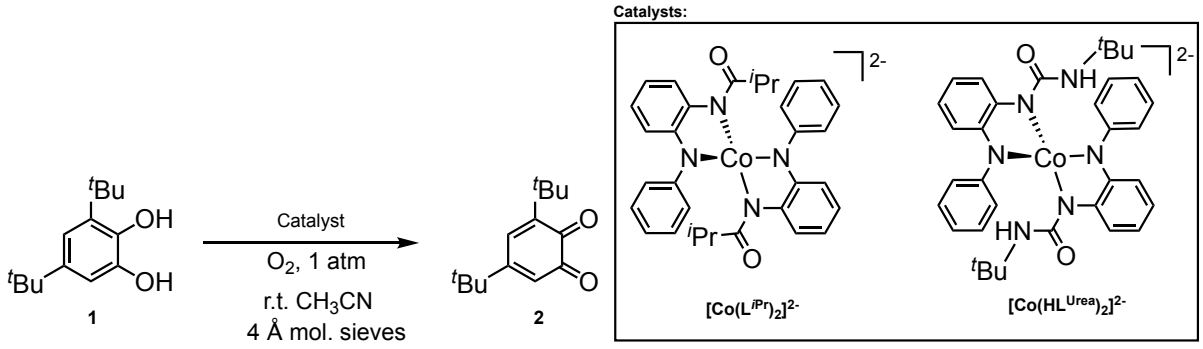

Entry	Catalyst	Time (hrs)	Cat.:Substrate Loading	% Conversion[a]	Isolated Yield of **2** (%)	TON
1	—	2	—	—	—	—
2	—	24	—	—	—	—
3	$CoBr_2$	2	1:150	—	—	—
4	$CoBr_2$	24	1:500	—	—	—
5	$(PPh_4)_2[Co(L^{iPr})_2]$	2	1:150	80	—	119[b]
6	$(PPh_4)_2[Co(HL^{Urea})_2]$	2	1:150	100	87	150[c]
7	$(PPh_4)_2[Co(L^{iPr})_2]$	24	1:500	63	—	313[b]
8	$(PPh_4)_2[Co(HL^{Urea})_2]$	24	1:500	100	—	499[b]

[a] % Conversions were determined via ^1H NMR
[b] TON = (moles of product determined from % conversion / moles of catalyst)
[c] TON = (moles of product / moles of catalyst)

2.7 Reactivity Studies of Phenolate Oxidative Coupling

Once we determined that our metal complexes were able to catalyze the 2-electron oxidation from catechol to quinone, we explored the possibility of our complexes catalyzing a 4-electron oxidation. The conversion of a phenolate to its corresponding quinone is a 4-electron process. This conversion is characteristic of tyrosinase activity.[22] Similar to catechol oxidase, tyrosinase is also a metalloenzyme in the copper type-III class of proteins.[23,24,25] We utilized aerobic substrate oxidation procedures and expected the product displayed in **Scheme 9**.

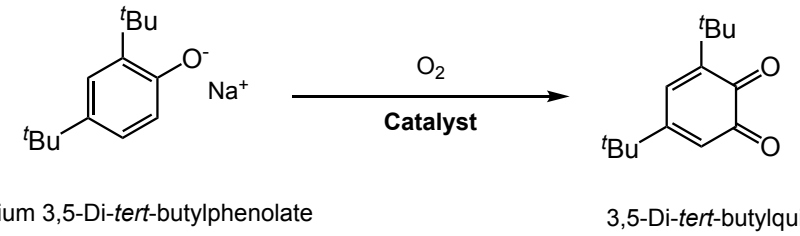

Sodium 3,5-Di-*tert*-butylphenolate

3,5-Di-*tert*-butylquinone

Scheme 9: Predicted oxidation of sodium 3,5-Di-*tert*-butylphenolate to 3,5-Di-*tert*-butyl-*o*-quinone.

Upon obtaining ^{1}H NMR of the product, we found that our complexes catalyzed the oxidative coupling of phenolate substrates. A new C-C bond was formed between two 3,5-Di-*tert*-butylphenolate substrates, resulting in a biphenyl product 3,3',5,5'-tetra-*tert*-butyl-[1,1'-biphenyl]-2,2'-diol. The formation of new C-C bonds has been reported difficult under mild conditions.[24-28] Our findings demonstrate aerobic oxidative phenolic coupling under ambient conditions. This reaction is likely an example of homo-coupling and likely is formed through a radical pathway.[8,29] Since the phenolate substrate contained two *tert*-butyl substituents, the variety of products that could be formed were limited. A problem with oxidative phenolic coupling is low selectivity.[30-34] Since biphenyl products are utilized in many drug products, selectivity of the reaction is important.[35] To date, we have minimal information on the selectivity of our complexes in catalyzing this reaction.

Oxidative phenolic coupling reactions were only conducted with cobalt(II) and copper(II) complexes because our past studies indicated the superior catalytic activity of these complexes when compared to zinc(II) complexes. Control reactions presented in Table 6 indicated that no reaction occurred without a metal complex. This data further corroborated finding that suggest $(PPh_4)_2[Co(HL^{Urea})_2]$ is our most reactive complex. Similar to findings from the oxidation of 3,5-DTBC, $(PPh_4)_2[Co(L^{iPr})_2]$ did not demonstrate as much catalytic activity as $(PPh_4)_2[Co(HL^{Urea})_2]$ when percent conversion of phenolate to biphenyl were compared. Additionally,

$(PPh_4)_2[Cu(L^{iPr})_2]$ had a lower percent conversion to the product than $K_2[Cu(HL^{Urea})_2]$. These findings indicate that incorporating hydrogen-bond donors into the redox-active ligand scaffold of cobalt(II) and copper(II) metal complexes enhance catalytic activity. Furthermore, cobalt(II) complexes $(PPh_4)_2[Co(HL^{Urea})_2]$ and $(PPh_4)_2[Co(L^{iPr})_2]$ displayed higher catalytic activity than copper(II) complexes $(PPh_4)_2[Cu(L^{iPr})_2]$ and $K_2[Cu(HL^{Urea})_2$. The results of the aerobic oxidative phenolic coupling reaction were consistent with past findings indicating that cobalt(II) complexes are more reactive than copper(II) complexes.

Table 6: Oxidative coupling of phenolates catalyzed by $[M(L^{iPr})_2]^{2-}$ and $[M(HL^{Urea})_2]^{2-}$.

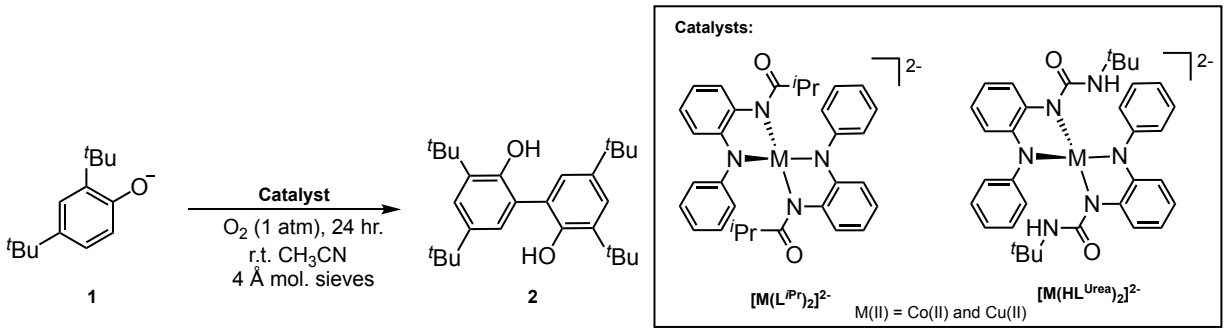

Entry	Catalyst	Cat.:Substrate Loading	% Conversion[a]
1	—	—	0[b]
2	$CoBr_2$	1:10	0[b]
3	$CuBr_2$	1:10	0[b]
4	$(PPh_4)_2[Co(L^{iPr})_2]$	1:10	77
5	$(PPh_4)_2[Co(HL^{Urea})_2]$	1:10	83
6	$(PPh_4)_2[Cu(L^{iPr})_2]$	1:10	21
7	$K_2[Cu(HL^{Urea})_2]$	1:10	63

[a] % Conversions calculated via ^1H NMR
[b] Only starting material was recovered

3. Conclusions and Future Directions

Ligands H_2L^{iPr} and H_3L^{Urea} have been synthesized and fully characterized. Through electrochemical investigation, the ligands have been shown to be redox-active. Cobalt(II), copper(II), and zinc(II) complexes supported by these redox active ligand scaffolds have also

been synthesized and characterized. Electrochemical data indicated that the cobalt(II) complexes were most easily oxidized. Additionally, the metal complexes supported by H_3L^{Urea} exhibited more negative redox potentials, indicating that hydrogen bond donors allowed for the complexes to be more easily oxidized. Cobalt(II), copper(II), and zinc(II) complexes were shown to be stabilized in four-coordinate distorted tetrahedral geometry by highly modular redox-active ligand scaffolds.

The mononuclear complexes were observed to facilitate catechol oxidation and oxidative coupling when exposed to molecular oxygen. Reactivity data obtained from the catalytic aerobic oxidation of 3,5-Di-*tert*-butylcatechol and 3,5-Di-*tert*-butylphenolate suggests that cobalt(II) complexes enhance catalytic activity more than copper(II) and zinc(II) complexes. Molecular sieves were able to enhance reactivity of the complexes. Additionally, metal complexes supported by H_3L^{Urea} displayed higher catalytic activity when compared to metal complexes supported by H_2L^{iPr}. These findings suggest that incorporating hydrogen-bond donors into the redox-active ligand scaffold enhances catechol oxidation and oxidative coupling. Reactivity data suggests that the mechanism of the catalysts may involve binding of the substrate to the metal center.

Future work will explore the mechanism of action of the $[M(L^{iPr})_2]^{2-}$ and $[M(HL^{Urea})_2]^{2-}$ complexes. Additional experiments should be carried out to determine the recyclability of the catalysts presented herein. Further work will be done to optimize the aerobic oxidation of 3,5-DTBC by $(PPh_4)_2[Co(HL^{Urea})_2]$. We will continue to explore our novel method of oxidative coupling. Other substrates including 3,5-Di-tert-butylphenol will be explored, as well as the ability for our metal complexes to catalyze the oxidative coupling of two different phenol molecules.

Nickel has recently been studied and has shown to be a robust first-row transition metal catalyst. This metal is readily abundant and has been shown to catalyze oxidation reactions.[36] Nickel complexes supported by H_2L^{iPr} and H_3L^{Urea} should also be explored, as well as their abilities to facilitate catechol oxidation and oxidative coupling.

4. Experimental

4.1. General Methods

All reagents and substrates utilized were purchased from commercial sources. Chemicals were utilized as purchased unless otherwise noted. Reagents utilized in the dry box were sparged under Argon. Substrates 3,5-di-*tert*butylcatechol (3,5-DTBC) and sodium 3,5-di-*tert*butylphenolate were purchased from Sigma Aldrich. The purity of the compounds was confirmed through ^{1}H NMR and GC before use. Elemental analyses were performed in the absence of oxygen by Atlantic Microlab, Inc., Norcross, GA. Varian INOVA 400 and VNMR 400 were used to record ^{1}H spectra at room temperature unless otherwise noted. Chemical shifts were reported in ppm and coupling constants were noted in Hz. Solution magnetic moments followed Evan's method and were taken in acetonitrile at room temperature. IR spectra were measured on a Varian Spectrophotometer. Cyclic voltammetry was conducted in dichloromethane with a 0.1 M tetrabutylammonium hexafluorophosphate ($TBAPF_6$) supporting electrolyte. Scanning was 10 mV/s. Cyclic voltammetry measurements were referenced against Fc/Fc^+ with Ag/Ag^+ as the reference electrode. Glassy carbon was the working electrode. These experiments were conducted using a CH Instruments (Austin, TX) Model 660C potentiostat. X-Ray crystal structures were obtained at the X-Ray Crystallography center at Emory University on a Bruker Smart 1000 CCD diffractometer. Solid-state infrared spectrophotometry experiments were carried out as KBr pellets using a Varian Scimitar 800 Series FTIR spectrophotometer. A

Cary50 spectrophotometer was utilized to obtain UV-visible absorption spectra with 1.0 path length quartz cuvettes.

4.2 Ligand Synthesis

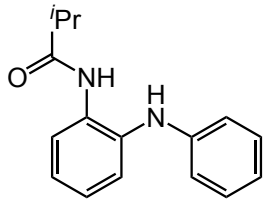

H_2L^{iPr}

Synthesis of H_2L^{iPr}: N-phenyl-*o*-phenylenediamine (4.7501 g, 0.02578 mol), was added to a solution of approximately 200 mL of dichloromethane. Next, 1.1 equivalents of triethylamine (3.955 mL, 0.02835 mol) was added to the solution via syringe. The solution stirred for approximately 30 minutes. The dark brown solution was placed in an ice bath and cooled to 0℃. 1.1 equivalents of 2-methylpropanoyl chloride (1.017 mL, 0.02835 mol) were added dropwise to the solution via syringe. The solution was allowed to stir overnight in the ice bath. Upon the addition of sodium bicarbonate to the solution, a clear layer and dark brown layer formed. The bottom dark brown layer was collected. The solution was filtered with dichloromethane and then a solution of sodium chloride was added, and an orange color was observed. The solution was allowed to stir while magnesium sulfate was added until solution turned purple. The mixture was allowed to stir for approximately 1 hour and the solution was filtered and the magnesium sulfate was removed. Solution was placed under vacuum to remove solvent and a brown-purple solid was recovered. The solid was dissolved in 1:6 dichloromethane:hexane solution. Solution was placed in the freezer overnight. The purple liquid was filtered through a frit. The filtrate was placed under vacuum. The product was isolated, resulting in a 74.8% yield of fine white powder.

^{1}H NMR (400 MHz $CDCl_3$) δ1.09 (d, 6H), δ2.42 (q, 1H), δ5.73 (s, 1H), δ 6.73 (d, 2H, J = 7.6 Hz), δ6.8 (t, 2H, J = 7.6 Hz), δ7.1, 7.24 (m, 5H), δ7.69 (s, 1H), δ7.97 (d, 1H).

*This compound was fully characterized by Dr. Savita Sharma.

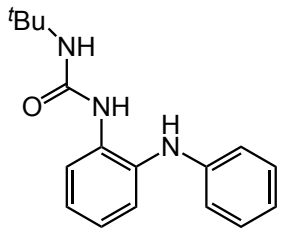

H_3L^{Urea}

Synthesis of H_3L^{Urea}: To prepare the redox-active ligand, N-phenyl-o-phenylenediamine (5.00 g, 0.0271 mol), was added to a solution of approximately 100 mL of methanol. A translucent dark red solution was formed. To this solution, tert-butyl isocyanate (3.09 mL, 0.0271 mol) was added through a syringe. This solution stirred for 24 hours and formed a translucent burgundy solution. The product was dried and stirred in hexanes. The product was collected in a filter frit and subsequently rinsed with hexane. The product was collected and dried under vacuum, yielding a fine white powder (93%). Product was confirmed using ^{1}H NMR. HRESI-MS: for $[H_3L^{Urea} +1]^-$ Calcd. 283.37 Found 284.00. FTIR (KBr, cm^{-1}): ν(CO) 1650, ν(NH) 3385, 3372, 3302.

*This compound was fully characterized by Dr. Omar Villanueva and Jessica Elinburg.

4.3 Metal Complex Synthesis

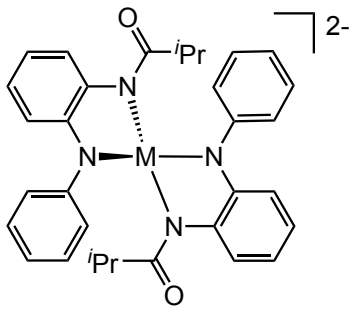

$[M(L^{iPr})_2]^{2-}$

General Procedure for Synthesis of $[M(L^{iPr})_2]^{2-}$: In a glove box under a nitrogen atmosphere, H_2L^{iPr} (0.3026g, 1.1897 mmol) was dissolved in approximately 4 mL of dimethylformamide resulting in a yellow solution. The solution was allowed to stir for approximately 5 minutes and then 2.0 equivalents of potassium hydride (96.00 mg, mmol) were added as a solid. The yellow mixture was allowed to stir to deprotonate for 1 hour. Next, a metal salt ($Cu(OAc)_2$, $CoBr_2$, or $ZnBr_2$) was added to the reaction mixture and allowed to stir for 3 hours. Next, 1.0 equivalents of PPh_4Br (0.4995g, mmol) was added to the mixture and was allowed to stir overnight. The solution was placed under vacuum to remove dimethylformamide. Approximately 8 mL of acetonitrile was added and the KBr was filtered out by a medium porosity filter frit. The filtrate was red and was recrystallized by the diffusion of diethyl ether into the solution containing acetonitrile.

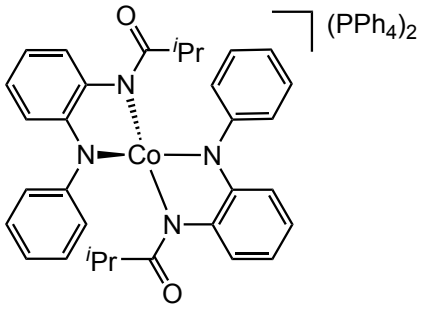

$(PPh_4)_2[Co(L^{iPr})_2]$

Synthesis of $(PPh_4)_2[Co(L^{iPr})_2]$: The general procedure for synthesis of $[M(L^{iPr})_2]^{2-}$ was carried out using $CoBr_2$ (30.1 mg, 0.138 mmol). After the addition of $CoBr_2$, the solution appeared to be dark red. Crystalline product was collected in a 71%. yield. ^1H NMR (400 MHz CD_3CN): (ppm) -65.578 (s), -58.062 (s), -1.825 (s), 56.565 (s), 72.0 (s), 81.231(s), 90.11(s).

*This complex was fully characterized by Dr. Savita Sharma.

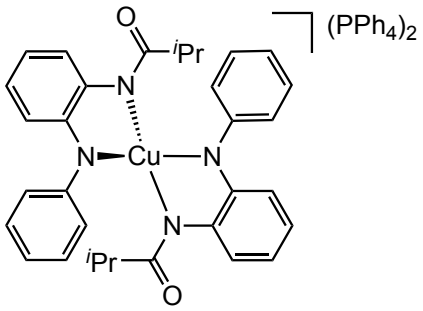

$(PPh_4)_2[Cu(L^{iPr})_2]$

Synthesis of $(PPh_4)_2[Cu(L^{iPr})_2]$: The general procedure for synthesis of $[M(L^{iPr})_2]^{2-}$ was carried out using $Cu(OAc)_2$ (110.0 mg, 0.606 mmol). The solution was deep green after the addition of $Cu(OAc)_2$. The crystalline product was collected and a 49% yield was obtained.

*This complex was fully characterized by Dr. Savita Sharma.

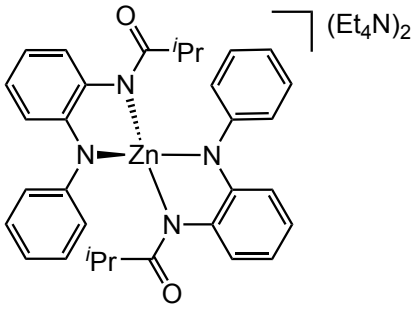

$(Et_4N)_2[Zn(L^{iPr})_2]$

Synthesis of $(Et_4N)_2[Zn(L^{iPr})_2]$: The general procedure for synthesis of $[M(L^{iPr})_2]^{2-}$ was carried out using $ZnBr_2$ (137.0 mg, 0.608 mmol). The crystalline product was collected in a 48% yield. HRESI-MS: for $[(Et_4N)_2[Zn(L^{iPr})_2]+1]^-$ Calcd. 519.2522 Found 520.24.

*This complex was fully characterized by Dr. Savita Sharma.

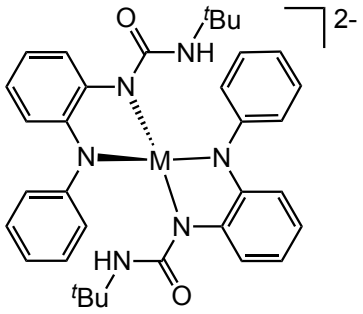

$[M(HL^{Urea})_2]^{2-}$

General Procedure for the synthesis of $[M(HL^{Urea})_2]^{2-}$: Under a nitrogen atmosphere, H_3L^{Urea} (0.500 g, 1.76 mmol) was dissolved in approximately 4 mL of dimethylformamide. This solution was allowed to stir for approximately 5 minutes and resulted in a translucent light purple solution. 2.0 equivalents of solid potassium hydride (0.141 g, 3.52 mmol) were added to the stirring solution. Hydrogen gas bubbles were present immediately upon the addition of the potassium hydride. This solution was allowed to stir for approximately 1 hour to allow the ligand to deprotonate. A reddish-brown solution resulted. To the reaction mixture, 0.5 equivalents of $M^{II}Br_2$ (M = Co, Cu, or Zn) salt (0.880 mmol). A color change occurs immediately when the

metal salt was added. Once the metal salt was added, reaction mixtures were allowed to stir overnight and then were dried. The crude product was redissolved in approximately 5 mL of acetonitrile to precipitate KBr as a byproduct. The mixture was allowed to stir for 30 minutes and then was passed through a medium porosity filter frit and KBr was isolated. The filtrate was placed under vacuum until a concentrated solution was obtained. The concentrated solution was recrystallized by layering with diethyl ether.

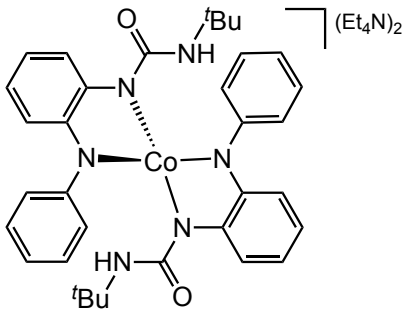

$(Et_4N)_2[Co(HL^{Urea})_2]$

Synthesis of $(Et_4N)_2[Co(HL^{Urea})_2]$: The general procedure for synthesis of $[M(HL^{Urea})_2]^{2-}$ was carried out using $CoBr_2$ (0.1152 g, 0.528 mmol). Approximately 1 hour after the addition of the metal salt, solid Et_4NBR (0.2219 g, 1.06 mmol) was added. The crystalline product was collected in a 66% yield. ^1H NMR (400 MHz CD_3CN): (ppm) -65.916(d), -59.307(s), -1.233(s), 55.070(s), 72.042(s), 82.527(s), 90.112(s).

*This complex was fully characterized by Dr. Omar Villanueva and Jessica Elinburg.

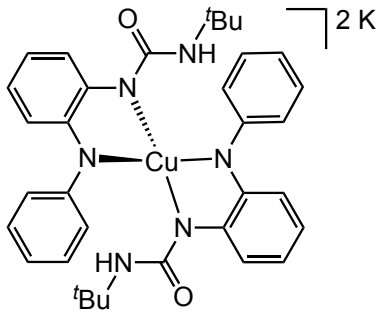

$K_2[Cu(HL^{Urea})_2]$

Synthesis of $K_2[Cu(HL^{Urea})_2]$: The general procedure for synthesis of $[M(HL^{Urea})_2]^{2-}$ was carried out using $CuBr_2$ (0.1222 g, 0.545 mmol). The crystalline product was collected in a 52% yield.

*This complex was fully characterized by Dr. Omar Villanueva and Jessica Elinburg.

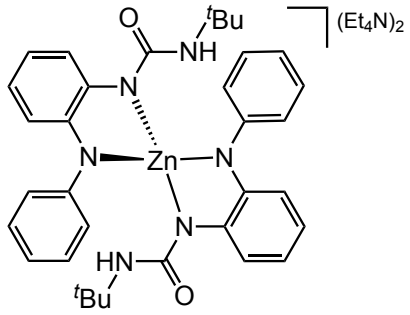

$(Et_4N)_2[Zn(HL^{Urea})_2]$

Synthesis of $(Et_4N)_2[Zn(HL^{Urea})_2]$: The general procedure for synthesis of $[M(HL^{Urea})_2]^{2-}$ was carried out using $ZnBr_2$ (0.0873 g, 2.17 mmol). Approximately 1 hour after the addition of the metal salt, solid Et_4NBR (0.2285 g, 1.09 mmol) was added. The crystalline product was collected in a 65% yield.

*This complex was fully characterized by Dr. Omar Villanueva and Jessica Elinburg.

4.4 Monitoring Aerobic Catechol Oxidation with UV-Visible Spectroscopy

Typical Catalytic Aerobic 3,5-di-tert-butylcatechol Oxidation UV-Visible Absorption Spectroscopy Procedure: Under a nitrogen atmosphere, a 0.0026 M solution of catalyst

($(PPh_4)_2[Co(HL^{Urea})_2]$ or $(PPh_4)_2[Co(L^{iPr})_2]$) was added to a 1.0 cm quartz cuvette (45 x 12.5 x 12.5 mm, 3.50 mL volume). A stir bar was placed in the cuvette and a septum was placed on the cuvette, which was sealed with electrical tape. 5 equivalents of catechol were added to a solution of acetonitrile and both solutions were removed from the dry box. 5 mL syringe was filled with O_2. The O_2 was injected into the headspace and the solution of catechol followed. The scan rate was 1 scan per minute for 60 minutes.

4.5 Catalytic Aerobic Substrate Oxidation

General Catalytic Aerobic Substrate Oxidation Procedure: Under a nitrogen atmosphere, a 25 mL Schleck flask was filled with 15 mg of metal complex dissolved in approximately 5 mL of acetonitrile. In trials noted, 4 Å activated molecular sieves were added to the reaction mixture in the dry box. A stir bar was added to the flask and was sealed with a rubber septa and black electrical tape. The solution was allowed to stir at room temperature while exposed to oxygen from a balloon for 15 minutes. 10, 50.0, 100.0, and 500.0 equivalents of substrate were massed depending on the trial and dissolved in approximately 5 mL of acetonitrile and was removed from the dry box. The substrate solution was added into the Schleck flask containing the metal complex once the Schleck flask was exposed to O_2 for 15 minutes. The substrates solution was added using a syringe and the rubber septa was punctured. The Schleck flask was removed from the oxygen after 2 or 24 hours depending on the trial. The stirring Schleck flask was placed under vacuum to remove the acetonitrile. 3-5 mL aliquots of a 9:1 hexane:ethyl mixture to extract the organic material. The solution was passed through a frit of silica. This was repeated until all organic material was removed from flask and then solution was placed under vacuum. Products were confirmed using ^1H NMR.

*This procedure was utilized for the substrates 3,5-Di-*tert*-butylcatechol and 3,5-Di-*tert*-butylphenolate.

5. References

1. Campbell, A.N.; Stahl, S.S. *Acc. Chem. Res.* **2012,** *45*, 851-863.
2. Anastas, P.T.; Kirchhoff, M.M.; Williamson, T.C. *Appl. Catal.* **2001**, *221*, 3-13.
3. Transition Metal Catalysis in the Pharmaceutical Industry. In *Applications of Transition Metal Catalysis in Drug Discovery and Development*, 1; Trost, B.M.; Crawley, M.L. John Wiley & Sons Inc.: Hoboken, New Jersey, 2012, pp 9-10.
4. Larsen, R.D., King, A.O., Chen, C.Y., Corley, E.G., Foster, B.S., Roberts, F.E., Yang, C., Lieberman, D.R., Reamer, R.A., Tschaen, D.M. and Verhoeven, T.R., *J. Org. Chem.* **1994**, *59*, 6391-6394
5. Chirik, P.J.; Wieghardt, K. *Science* **2010,** *327*, 794-795.
6. Vidossich, P.; Ujaque, G.; Lledós, A. *Chem. Comm.* **2012**, *48*, 1979-1981.
7. Moore, W.; Hysell, D.; Hall, L.; Campbell, K.; Stara, J. *Environ. Health Perspect*. **1975**, *10*, 63.
8. Lee, Y.E.; Cao, T.; Torruellas, C.; Kozlowski, M.C. *J. Am. Chem. Soc.* **2014**, *136*, 6782-6785.
9. Yasbin, R.E.; Matthews, C.R.; Clarke, M.J. *Chem. Biol. Int.* **1980**, *31*, 355-365.
10. Mukherjee, S.; Weyhermüller, T.; Bothe, E.; Wieghardt, K.; Chaudhuri, P. *Dalton Trans.* **2004**, 22, 3842-3853.
11. Neves, A.; Rossi, L.M.; Bortoluzzi, A.J.; Szpoganicz, B.; Wiezbicki, C.; Schwingel, E.; Haase, W.; Ostrovsky, S. *Inorg. Chem.* **2002**, *41*, 1788-1794.

12. Que Jr, L.;Tolman, W.B. *Nature*, **2008** *455*, 333.

13. Koval, I.A., Gamez, P., Belle, C., Selmeczi, K. and Reedijk, J. *Chem. Soc. Rev.* **2006**, *35*, 814-840.

14. Torelli, S.; Belle, C.; Hamman, S.; Pierre, J.L.; Saint-Aman, E. *Inorg. Chem.* **2006**, *41*, 3983-3989.

15. Borovik, A.S. *Acc. Chem. Res*. **2005**, *38*, 54-61.

16. Majumder, S.; Mondal, S.; Lemoine, P.; Mohanta, S. *Dalton Trans.* **2013**, *42* 4561-4569.

17. Mendoza-Quijano, M.R.; Ferrer-Sueta, G.; Flores-Álamo, M.; Aliaga-Alcalde, N.; Gómez-Vidales, V.; Ugalde-Saldívar, V.M.; Gasque, L. *Dalton Trans*. **2012**, *41*, 4985-4997.

18. Ketterer, N.A.; Fan, H.; Blackmore, K.J.; Yang, X.; Ziller, J.W.; Baik, M.H.; Heyduk, A.F. *J. Am. Chem. Soc.* **2008**, *130*, 4364-4374.

19. Collins, T. J., *Acc. Chem. Res.* **1994,** *27*, 279.

20. Sharma, S.K.; May, P.S.; Jones, M.B.; Lense, S.; Hardcastle, K.I.; MacBeth, C.E., *Chem. Comm.* **2011**, *47*, 1827-1829.

21. Yang, L.; Powell, D.R.; Houser, R.P. *Dalton Trans.* **2007**, 9, 955-964.

22. Shaban, S.Y.; Ramadan, A.E.M.M.; Ibrahim, M.M.; Mohamed, M.A.; van Eldik, R. *Dalton Trans.* **2015**, *44*, 14110-14121.

23. Ayad, M.I. *Arabian Journal of Chemistry*, **2016**, *9*, S1297-S1306.

24. Dyadyuk, A.; Sudheendran, K.; Vainer, Y.; Vershinin, V.; Shames, A.I.; Pao, D. *Org. Lett.* **2016**, *18*, 4324-4327.

25. Hassan, J.; Sevignon, M.; Gozzi, C.; Schulz, E.; Lemaire, M. *Chem. Rev.* **2002**, *102*,1359-1470.

26. Mukhopadhyay, S.; Ratner, S.; Spernat, A.; Qafisheh, N.; Sasson, Y. *Org. Process Res. Dev.* **2002**, *6*, 297-300.

27. Chen, X.; Engle, K.M.; Wang, D.H.;Yu, J.Q. *Angew. Chem. Int. Ed,* **2009***, 48*, 5094-5115.

28. Funes-Ardoiz, I.; Maseras, F. *ACS Catal.* **2018**, *8*, 1161-1172.

29. Qin, G.; Chen, X.; Yang, L.; Huang, H. *ACS Catal.* **2015**, *5*, 2882-2885.

30. Šmejkalová, D.; Piccolo, A.; Spiteller, M. *Environ. Sci. Tech.* **2006**, *40*, 6955-6962.

31. Shalit, H.; Libman, A.; Pao, D. *J. Am. Chem. Soc.* **2017**,*139*,13404-13413.

32. Papouchado, L.; Petrie, G.; Adams, R.N. *J. Electroan. Chem. Interf. Electrochem.* **1972**, *38*, 389-395.

33. Barrett, T.N.; Braddock, D.C.; Monta, A.; Webb, M.R.; White, A.J. *J. Nat. Prod.* **2011**, *74*, 1980-1984.

34. Lim, P.K.; Cha, J.A.; Patel, C.P. *Ind. Eng. Chem. Process Des. Dev.* **1983**, *22*, 477-482.

35. Quell, T.; Hecken, N.; Dyballa, K.M.; Franke, R.; Waldvogel, S.R. *Org. Process Res. Dev.* **2016**, *21*, 79-84.

36. Deb, T.; Rohde, G.T.; Young Jr, V.G.; Jensen, M.P. *Inorg. Chem.* **2012** *51*, 7257-7270.